Coupling Strategies for Large Industrial Models

Jens Neumann and Wolf Krüger

Institute of Aeroelasticity,
Bunsenstrasse 10, 37075 Göttingen, Germany
{jens.neumann,wolf.krueger}@dlr.de

Abstract. In this article an investigation of possible coupling strategies for large numerical models in fluid-structure interaction is given. The focus is on the development and the assessment of a simplified approach that uses existing and well verified scattered data interpolation methods. The interpolation problem is addressed by a pragmatic partitioning approach of large models. Analysis of the interpolation of deflections between different discretization of the coupling models are performed, together with comparisons of static fluid-structure simulations with measured data of the elastic DLR-F12 wind tunnel model. The loads transfer between CFD mesh and FE model for different partitioning schemes is performed and assessed, finally some considerations for the use of the suggested strategies on large models are presented.

Keywords: fluid-structure interaction for large models, scattered data interpolation, spatial partitioning approaches, load transfer.

1 Introduction

Aeroelastic analysis generally implies the interaction between a flow field around an elastic structure and the reverse influence of the structural deformation on the flow. One important aspect of this problem is the spatial coupling between the numerical models of flow and structure. Usually, the discretization of these two models can be of a complete different type. For the calculation of transonic flow, computational fluid dynamics (CFD) is a standard approach. Here, the mathematically discretization of the flow field is based on a finite volume approach. For the calculation of the deformations of the elastic structure, finite element (FE) modelling is common.

The differing discretization for flow and structure leads to an interpolation problem between the two models. If an interpolation matrix H exists, then the deformations u_a of the aerodynamic surface mesh can be interpolated from structural deformations u_s by using Eq. 1, see [1]

$$u_a = H u_s. \tag{1}$$

Likewise, the aerodynamic forces f_a can be transformed to structural forces f_s using the transposed of the coupling matrix H by Eq. 2, see also [1]

$$f_s = H^T f_a. \tag{2}$$

N. Kroll et al. (eds.), *Computational Flight Testing*, Notes on Numerical Fluid Mechanics and Multidisciplinary Design 123,
DOI: 10.1007/978-3-642-38877-4_14,

Eq. 2 guarantees the global equilibrium of forces and momentum as well as balance of the virtual work on both sides.

In the project COMFLITE, so-called scattered data interpolation methods with radial basis functions, see [2] or [3], have been used for the calculation of the interpolation matrix H. Examples for scattered data interpolation with different radial basis functions applied for fluid structure interaction are given in [1] and [4]. Radial basis functions can be divided in two types, those with a global and those with a local character concerning the influence area of the interpolation function. Radial basis functions with a global influence area include the thin plate spline [5] and the volume spline [6]. Radial basis functions with local character use a so-called compact support radius, see [7]. Those functions can exclude the global influence of interpolation points between parts on the structure which are far away from each other, like the influence of the deflections of the horizontal tail plane on the deflections of the wing.

One of the problems for large industrial models, like whole aircraft configurations, is the dimension of the interpolation problem. In [8] the build-up of the interpolation matrix H has been described as of an $O(N^3)$ complexity with $O(MN^2)$ operations. Here, N denotes the number of supporting points and M the number of the interpolation points. The size of the interpolation matrix H is $M^{cfd} \times N^{fe}$, where N^{fe} usually is a certain subset of the nodes of the structure model (FE model) and M^{cfd} the number of the aerodynamic surface points of the CFD model. Thus, for fine CFD meshes and FE grids, resulting in a high number of coupling points, the coupling matrix quickly becomes too large for the available computer memory and can therefore not be calculated. Moreover, for large model problems the computation time of the matrix will increase with increasing number of M and N to an extend which is not reasonable.

In the literature there are examples for the handling of large interpolation problems. One example is the use of a so-called "Partition of Unity" approach, see [9]. In [8] and [10] the approach has been applied to structures relevant for aircraft and aeronautical applications. In [11], a similar concept to divide the interpolation region has been used. But neither one of the approaches has been systematically investigated concerning the influence of the number and the directions of the partitions, nor have respective simulation results been compared to experimental data.

The aim of this paper is to describe the development and application of a simplified partitioning approach for the spatial interpolation problem illustrated above. Both the interpolation of deflections and the loads transfer are investigated. For interpolation of deflections, the coupling regions will be divided into equidistant partitions in a defined Cartesian direction, e.g. the x-direction, with equal overlapping regions. In each overlapping region so-called Hermite polynomial functions are used in order to smooth multiple interpolated values. For the loads transfer, non-overlapping regions are suggested. The influence of the number as well as of the directions of the partitions will be investigated systematically. Finally, the analysis results will be compared with experimental data.

2 Scattered Data Interpolation with Radial Basis Functions

In this section, some general considerations about the scattered data interpolation function will be introduced. The general interpolation function reads

$$f(x_j) = \alpha_1 + \alpha_2 x_i + \alpha_3 y_i + \alpha_4 z_i + \sum_{j=1}^{N} \beta_j \varphi\left(\|x\|_{ij}\right) \tag{3}$$

with the basis function $\varphi\left(\|x\|_{ij}\right)$. The radial basis function is a function of the euclidean distance $\|x\|_{ij}$ of a supporting point x_i to the interpolation point x_j

$$\|x\|_{ij} = \sqrt{(x_i - x_j)^2 + (y_i - y_j)^2 + (z_i - z_j)^2}. \tag{4}$$

Considering unit displacements for the solution vector $f(x_j)$ the interpolation problem leads to an equation system with the unknown coefficients α and β that has to be solved

$$\begin{bmatrix} 0 & A \\ A^T & \varphi \end{bmatrix} \cdot \begin{bmatrix} \alpha \\ \beta \end{bmatrix} = \begin{bmatrix} 0 \\ E \end{bmatrix}$$

with the following matrices

$$A = \begin{bmatrix} 1 & 1 & \cdots & 1 \\ x_1 & x_2 & \cdots & x_i \\ y_1 & y_2 & \cdots & y_i \\ z_1 & z_2 & \cdots & z_i \end{bmatrix}; \qquad \varphi = \begin{bmatrix} \varphi_{11} & \varphi_{12} & \cdots & \varphi_{1i} \\ \varphi_{21} & \varphi_{22} & \cdots & \varphi_{2i} \\ \vdots & \vdots & \ddots & \vdots \\ \varphi_{i1} & \varphi_{i2} & \cdots & \varphi_{ii} \end{bmatrix}; \qquad E = \begin{bmatrix} 1 & 0 & \cdots & 0 \\ 0 & 1 & \cdots & 0 \\ \vdots & \vdots & \ddots & \vdots \\ 0 & 0 & \cdots & 1 \end{bmatrix}.$$

The calculation of the unknown coefficients is carried out with

$$\begin{bmatrix} \alpha \\ \beta \end{bmatrix} = \begin{bmatrix} 0 & A \\ A^T & \varphi \end{bmatrix}^{-1} \cdot \begin{bmatrix} 0 \\ E \end{bmatrix}$$

After the determination of the unknown coefficients the interpolation matrix H can be calculated by

$$[H] = \begin{bmatrix} B & C \end{bmatrix} \cdot \begin{bmatrix} \alpha \\ \beta \end{bmatrix}$$

with the following matrices

$$B = \begin{bmatrix} 1 & x_1 & y_1 & z_1 \\ 1 & x_2 & y_2 & z_2 \\ 1 & \vdots & \vdots & \vdots \\ 1 & x_j & y_j & z_j \end{bmatrix}; \qquad C = \begin{bmatrix} \varphi_{11} & \varphi_{12} & \cdots & \varphi_{1i} \\ \varphi_{21} & \varphi_{22} & \cdots & \varphi_{2i} \\ \vdots & \vdots & \ddots & \vdots \\ \varphi_{j1} & \varphi_{j2} & \cdots & \varphi_{ji} \end{bmatrix}.$$

With this interpolation matrix H the vector of the unknown displacements of the aerodynamic surface points u_a can then be calculated on the basis of the structural displacements u_s from a finite element solution with Eq. 1.

2.1 Global and Local Radial Basis Functions

As mentioned above, global and local radial basis functions can be distinguished. The influence of a global basis function φ on the interpolation area is completely unlimited. Each value of a supporting point thus has an influence on the interpolation points. As a result, the calculated interpolation matrix can become very large, and it is completely loaded. For large industrial models the interpolation matrix H can thus exceed the memory of the architecture, as described in the section above. Examples for global basis functions are the Volume Spline (Eq. 5) and the Thin Plate Spline (Eq. 6.),

$$\varphi\left(\|x\|_{ij}\right) = \|x\|_{ij} \tag{5}$$

$$\varphi\left(\|x\|_{ij}\right) = \|x\|_{ij}^2 \, log \, \|x\|_{ij} \tag{6}$$

Local basis functions φ_r have an influence area which is driven by a so-called compact support radius. Here, the influence area of a supporting point P_i to an interpolation point P_j is restricted through a radius r. In 2-dimensional space the influence area is a circle, in 3-dimensional space it is a sphere. The compact support radius r controls the influence of the basis function. In consequence, the interpolation matrix can become sparse, also reducing the calculation time for the generation of the matrix.

Examples for local basis functions (with compact support radius) are the Euclid's Hat function,

$$\varphi_r\left(\|x\|_{ij}\right) = \pi\left(\left(\frac{1}{12}\|x\|_{ij}^3\right) - \left(r^2\|x\|_{ij}\right) + \left(\frac{4}{3}r^3\right)\right) \tag{7}$$

$$\varphi_r\left(\|x\|_{ij}\right) = 0 \qquad \{\forall \|x\|_{ij} \geq 2r\} \tag{8}$$

3 Used Coupling Process Chains

In the project COMFLITE, two essential coupling approaches have been established for fluid structure interaction simulations. The first one is the so-called "discrete approach", based on structural models described in physical coordinates, the second one is the modal approach, using a modal transformation of the general equation of motion, expressed in generalized coordinates. One major difference between the two approaches lies in the spatial coupling. The discrete approach uses the coupling matrix H in order to interpolate the discrete displacements from structural nodes according to Eq. 1. Likewise, the transposed matrix H^T can be used to transform the aerodynamic forces on the structural nodes according to Eq. 2. These coupling steps have to be done in each iteration step, see the left flow chart in Fig. 1.

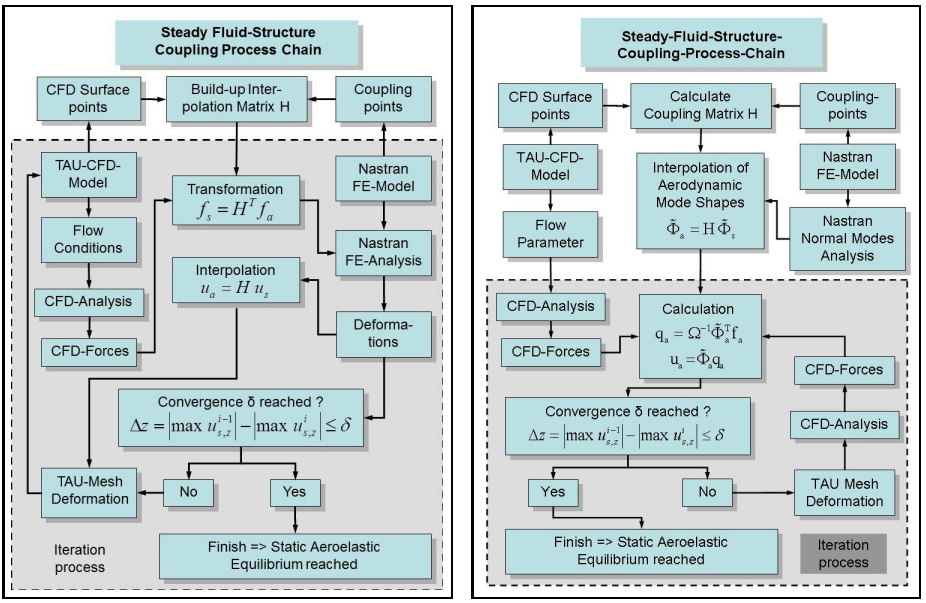

Fig. 1. Left: Process chain of discrete approach. **Right:** Process chain of modal approach.

Unlike the discrete approach, the modal approach uses the coupling matrix H only once. The general equation of motion in generalized coordinates reads

$$\{\ddot{q}(t)\} + [\Omega]\{q(t)\} = \left[\tilde{\Phi}\right]^T \{f_s(t)\}\,. \tag{9}$$

Introducing now the linear approach for the transformation of the aerodynamic loads according to Eq. 2 in Eq. 9 results in

$$\begin{aligned}\{\ddot{q}(t)\} + [\Omega]\{q(t)\} &= \left[\tilde{\Phi}\right]^T [H]^T \{f_a(t)\} \\ &= \left[\tilde{\Phi}_a\right]^T \{f_a(t)\}\,.\end{aligned} \tag{10}$$

Now, on the right hand side of Eq. 10, the aerodynamic forces acting on the surface of the system, and the structural eigenvalues $\tilde{\Phi}_s$, are interpolated onto the aerodynamic surface mesh. This interpolation has to be done only once and can be performed as a pre-processing step before the coupling procedure by

$$\left[\tilde{\Phi}_a\right] = [H]\left[\tilde{\Phi}_s\right] \tag{11}$$

where $\tilde{\Phi}_a$ denotes the modal matrix on the aerodynamic surface grid containing the interpolated real mode shapes of the structure $\tilde{\Phi}_s$. Note, that all mode shapes

$\tilde{\Phi}_s$ have to be normalized to a generalized mass of "1". For steady state problems, like the calculation of the static aeroelastic equilibrium, Eq. 10 reduces to

$$\{q\} = [\Omega]^{-1} \left[\tilde{\Phi}_a\right]^T \{f_a\}\,. \tag{12}$$

The displacements of the aerodynamic surface points can then be calculated by

$$\{u_a\} = \left[\tilde{\Phi}_a\right] \{q\}\,. \tag{13}$$

The applied coupling process chain for the modal approach can be seen in the right flow chart of Fig. 1. The modal approach has been successfully used for fluid-structure interaction simulation in [12] and [13].

4 Partitioning Approach for Large Industrial Models

For the handling of large industrial models, it is suggested to treat the interpolation problem in partitions. A simple partitioning approach can be described as follows. For a global coupling, the coupling matrix H usually covers the complete interpolation region, i.e. the aerodynamic surface points and the underlying structural nodes of the considered model. However, it is also possible to divide the coupling region in n areas Ω_i $(i = 1...n)$ and to calculate a separate coupling matrix for each area H^{Ω_i}. For the discrete approach and the calculation of the structural forces this still guarantees that the global equilibrium of forces and momentum, ensured for the global coupling by Eq. 2, is now also ensured for each coupling matrix H^{Ω_i} and therefore also for each local partition

$$f_s^{\Omega_i} = \left(H^{\Omega_i}\right)^T f_a^{\Omega_i} \tag{14}$$

and

$$\sum f_s = \sum f_a = \sum_{i=1}^{n} f_s^{\Omega_i}. \tag{15}$$

However, for the interpolation of displacements, the division of the interpolation region would produce discontinuities in the interpolated areas from one partition Ω_i to its neighbor partition Ω_{i+1}. This is true both for the discrete approach, Eq. 1, and for the modal approach using Eq. 11 in order to interpolate the structural mode shapes onto the aerodynamic surface. As a solution, in this areas it is advisable to define overlapping regions and to smooth the interpolated values in the overlap. Therefore, the use of so-called weighting functions, which in sum give the "1"

$$w_1(\xi) + w_2(\xi) = 1 \qquad \text{with } \xi = x/l. \tag{16}$$

will be used. The applied weighting functions are the so-called Hermite-Polynomial functions, see the left graph in Fig. 2, and they are

$$w_1(\xi) = 1 - 3\xi^2 + 2\xi^3 \tag{17}$$

$$w_2(\xi) = 3\xi^2 - 2\xi^3. \tag{18}$$

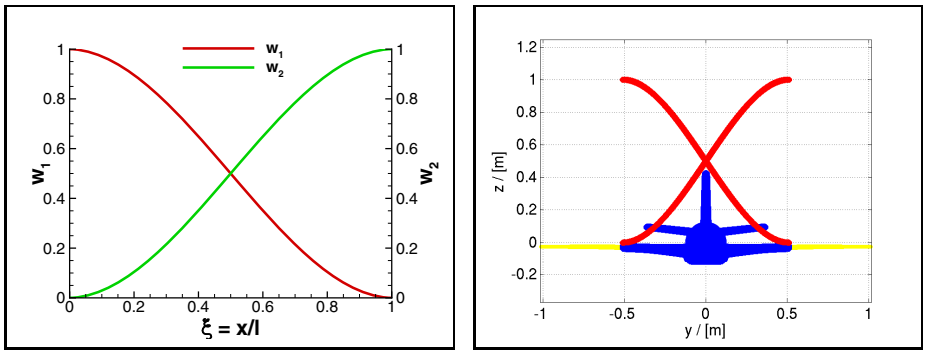

Fig. 2. Left: Curves of the Hermite-Polynomial functions. **Right:** Coupling regions for two partitions and influence area (blue) of the weighting functions (red).

For the applied approach the subareas can be divided automatically in equidistant parts in x-, y- or z-direction with overlapping regions of e.g. 50%. Exemplarily, in the right graph in Fig. 2, for two partitions, the overlapping areas (blue lines) and the influence area of the applied weighting functions (red lines) are depicted.

5 Test of the Partitioning Approach for Deflections

In the following subsection, the influence of the number of partitions on the quality of the resulting interpolation is assessed. The partitioning approach has been tested using the finite element model of the DLR-F12 configuration. The DLR-F12 configuration is a wind tunnel model of a conventional passenger aircraft including wing, fuselage and tail. The FE model has been built up in ANSYS, with approximately 100000 nodes. The model is a good test case for the coupling strategies as the FE model has a very fine geometrical resolution, particularly on the surface. For the validation of the interpolation scheme, a reference solution for the deflections has been obtained using the results of a selected mode shape calculated on the complete structural mesh. In the next step, the same mode shape is represented by a subset of nodes. The surface representation of the mode shapes to be compared to the reference solution is obtained by interpolating the remaining surface nodes, which are not part of the subset, based on the mode shape information of the nodes in the subset. For the test, mode shape no. 19 has been selected because it involves a lot of local motion on the complete aircraft, see the left graphic in Fig. 3. A subset of the existing FE nodes defined as coupling nodes can be seen in the right graphic in Fig. 3. For the test of the partitioning approach 1126 FE nodes are used which are more or less equally distributed over the whole region.

The approach is tested for one up to fifty partitions, using always 50% overlap per coupling region. Divisions have been performed in x-, y-, and z-direction, respectively. For each interpolated mode shape the MAC-values according to Eq. 19

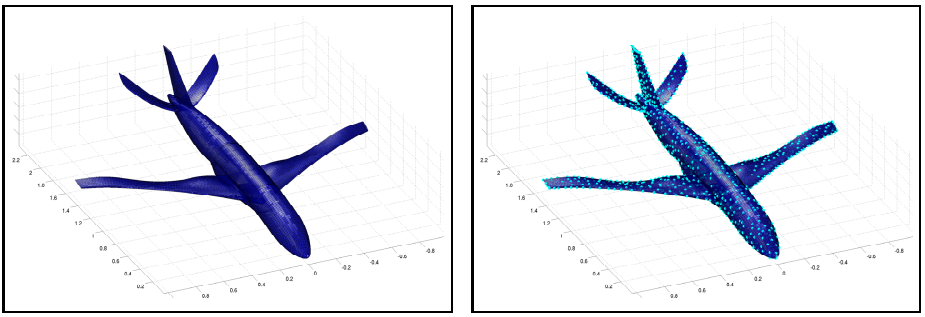

Fig. 3. Left: Mode shape No.19. **Right:** FE-Model of the DLR-F12 model and 1126 chosen nodes as coupling points (cyan).

are calculated. The calculated MAC-values will quantify the agreement between the reference mode shape (i.e. eigenvector) of the FE model and the interpolated mode shape based on the subset. Values of 1 mean that the eigenvectors match perfectly, i.e. 100%.

$$MAC_{ij} = \frac{\left(\{\Psi\}_i^T \cdot \{\Phi\}_j\right)^2}{\left(\{\Psi\}_i^T \cdot \{\Psi\}_i\right)\left(\{\Phi\}_j^T \cdot \{\Phi\}_j\right)} \tag{19}$$

$\{\Psi\}_i$: $\quad$ i$^{\text{th}}$ eigenvector of complete FE model from normal modes analysis
$\{\Phi\}_j$: $\quad$ j$^{\text{th}}$ interpolated eigenvector of the same FE model based on a subset of FE nodes

In Eq. 19, Ψ_i denotes the i$^{\text{th}}$ eigenvector of the FE model obtained from an eigenvalue analysis, e.g. by ANSYS or NASTRAN. Φ_j denotes the j$^{\text{th}}$ interpolated eigenvector of the same FE model using the scattered data interpolation method described above and the introduced partitioning approach. For each partition the "Thin Plate Spline" function is used as radial basis function.

The results for this investigation are plotted in Fig. 4. With increasing number of partitions in z-direction the agreement between interpolated and reference eigenvector increases equally. For partitions in x-direction the accuracy decreases slightly. Nevertheless, it is recognizable that the range of the MAC-values between $99.8\% < \text{MAC} < 99,95\%$ is very satisfying. The method works very well and the dependance of the partitioning approach on the number of partitions is not very significant. Thus, the number of partitions used for the interpolation of eigenvalues according to Eq. 11 does not influence the interpolation results significantly, or, in other words, results of a coupled simulations are expected to be almost independent from the number of chosen partitions.

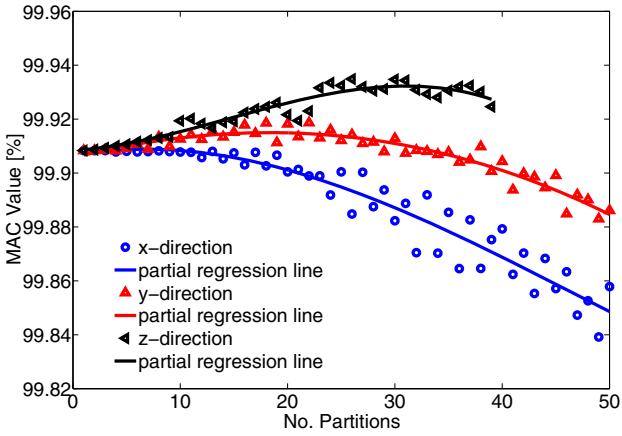

Fig. 4. MAC-Values for different partition directions and their dependency of the number of partitions

6 Coupled Simulations of the DLR-F12

In this section the suggested partitioning approach will be tested in coupled simulations using the modal approach in order to calculate the static aeroelastic equilibrium of the DLR-F12 wind tunnel model. The wind tunnel tests have been performed in order to provide an experimental data basis for code validation of tools for the prediction of the static aeroelastic equilibrium as well as the investigation of dynamic derivatives in flight maneuvers, see [14] and [15]. The wind tunnel tests have been conducted in the low-speed wind tunnel in Braunschweig (NWB) under guidance of the DLR Institute of Aerodynamic and Flow Technology in Braunschweig.

The used finite element model of the DLR-F12 for the presented coupled simulations has been introduced in Section 5. For the calculation of the aeroelastic equilibrium with the modal approach, the first 20 mode shapes of the complete structural model have been interpolated onto the aerodynamic surface mesh of the corresponding CFD model. The used CFD mesh of the DLR-F12 model is depicted in the left graph in Fig. 5. The mesh has 12.4 million points and 31.6 million elements. The boundary layer has been resolved with 28 layers and 20.8 million prisms.

For the calculation of the aerodynamic forces, the three-dimensional and time accurate Reynolds-Averaged Navier-Stokes (RANS) equations have been solved with the DLR-TAU-Code [16]. For the spatial discretization a centered scheme with scalar artificial dissipation was used in combination with a backward Euler implicit scheme solved with LU-SGS iterations [17], using local time stepping for the integration of the discrete equations. For the calculation of the viscous fluxes the one-equation Spalart-Allmaras turbulence model [18] in original version was used to taking into account the turbulence's in the flow field.

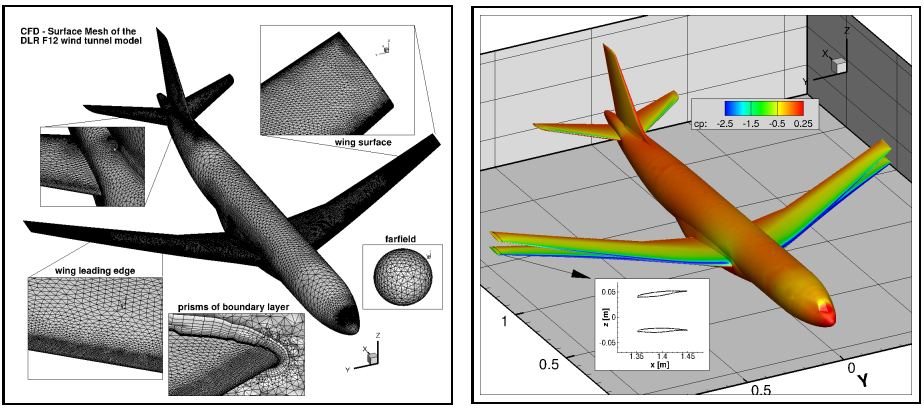

Fig. 5. Left: CFD mesh of the DLR-F12 wind tunnel model. **Right:** Deformation and c_p-distribution in static aeroelastic equilibrium state for an angle of attack $\alpha_0 = 8.0$deg.

Four coupled calculations will be compared. The first is the coupled simulation using just one partition and therefore only one interpolation matrix H. For this calculation the chosen coupling nodes of the FE model, which are the supporting points for the interpolation, were reduced to 1126 points continuously distributed over the whole model, in order to make the interpolation feasible at all. The second calculation has been carried out by using less FE model information (199 points) and three partitions in x-direction in order to interpolate the mode shapes onto the aerodynamic mesh. The third simulation has been conducted by using 1126 points and 20 partitions, with the partitions being evenly spaced in y-direction. In the fourth calculation, 43422 points have been used, the coupling region has been divided into 200 equidistant partitions in y-direction.

In all calculations the overlapping regions have been kept constant, always covering 50% of the neighbouring partition. In Table 1 the variations of the parameters for the partitioning approaches are listed.

Table 1. Partitioning parameters for calculations

No.	Coupling-Points	Parts	Direction	Overlap	Basis Function
1	1126	1	-	50%	Thin Plate Spline
2	199	3	x	50%	Thin Plate Spline
3	1126	20	z	50%	Thin Plate Spline
4	43244	200	y	50%	Thin Plate Spline

In Table 2 the significant aerodynamic flow parameters for the simulations are listed. All calculations have been carried out at the same flow parameters. The only changes which have been conducted were the variation of the partitioning parameters according to Table 1. Criteria for the evaluation of the quality of the

Table 2. Aerodynamic parameters for calculations

Parameter	Value	Unit
Mach number	0.205723	$[-]$
Reynolds number	1.28e+06	$[-]$
reference chord length	0.252625	$[m]$
reference density	1.22523	$[kg/m^3]$
reference velocity	70.0	$[m/s]$
reference temperature	288.15	$[K]$
angle of attack	8.0	$[deg.]$

different interpolation approaches are the comparison of the resulting pressure distributions on the wing, as well as the comparison of the wing deflections.

In the right graphic in Fig. 5 above the c_p-distributions for the undeformed model and the model in aeroelastic equilibrium state are depicted. The results of all simulations, compared to the experimental data for the pressure coefficients c_p, are depicted in Fig. 6. There were two measurement sections on the model for the recording of the pressure coefficients c_p, one on the left wing at $y = -0.457m$ and one on the right wing at $y = 0.457m$. As can be seen in Fig. 6, neither on the left nor on the right wing there is a significant difference between the measured and the calculated pressure distributions. Furthermore, the pressure coefficients with respect to the variation of the number and the direction of the partitions differ only marginally.

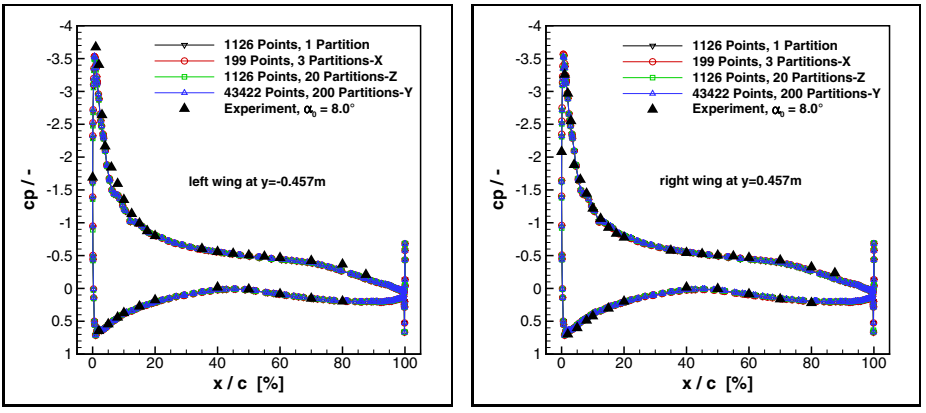

Fig. 6. Left: Comparison of measured and calculated cp-distributions for left wing. **Right:** Comparison for right wing.

In Fig. 7 the comparisons with respect to the elastic deformations of the DLR-F12 wind tunnel model at an angle of attack of $\alpha_0 = 0.8deg$ are depicted. The elastic bending deformation has been compared for the c/4-line along the span of

the left wing and is denoted with the letter w. It can be observed that the maximum elastic deformation w hardly differs between the four interpolation variations. The maximum deviation between the approaches is $\Delta w_{max} \sim 0.35mm$. The same can be observed for the elastic twist, denoted as $\Delta\epsilon$, representing the change in the local incidence angle α of the model. For that case, the deviation between the cases is $\Delta\alpha_{max} \sim 0.1deg$ and can thus also be considered negligible. Furthermore, all results match well with the measured data.

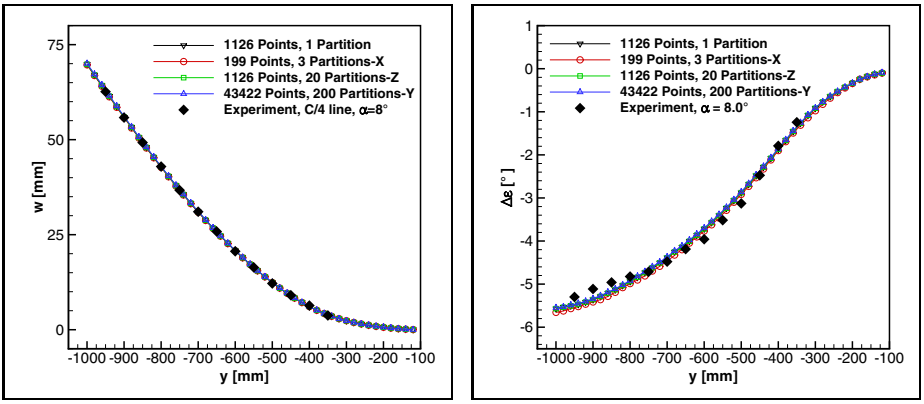

Fig. 7. Left: Comparison of measured and calculated displacements with and without partitioning approach. **Right:** Comparison of measured and calculated elastic twist.

Summarizing, the results show the functionality of the partitioning approach. For the DLR-F12 configuration chosen as an example, neither the partitioning direction nor the number of partitions, and therefore the number of applied coupling matrices, significantly influence the results of the static aeroelastic equilibrium.

7 Applied Partitioning Approach for Load Transformation

In the following section, the load transfer, i.e. the conversion of the load from the CFD mesh to the FE nodes, is analyzed. Special focus is on the resulting local load distribution and momentum. The same partitioning procedure as used for the interpolation of the deflection can be applied for the load transformation according to Eq. 2. However, as already mentioned in Section 4, for the load transfer it is not necessary to generate overlapping regions among the partitions. Rather, it is advantageous to keep the partitions without overlapping regions, as smoothing the values in potential overlaps can disturb the equilibrium of forces and momentum for the actual partition.

In Fig. 8 the c_p-distribution and the corresponding forces of the DLR-F12 model in aeroelastic equilibrium, obtained from the coupled calculation described

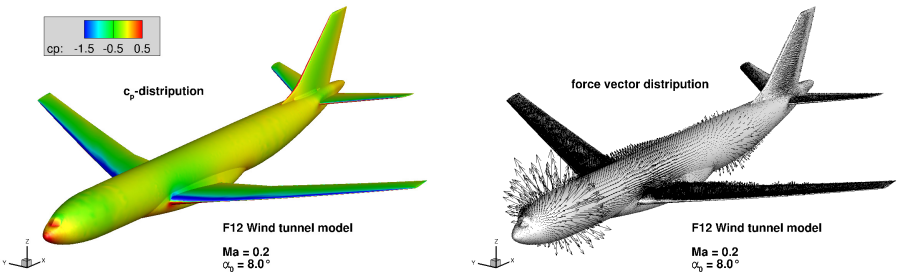

Fig. 8. Left: c_p-distribution in aeroelastic equilibrium. **Right:** Corresponding force distribution.

in Section 6, is shown. As a test case, the corresponding loads are transformed using at first 199 coupling points and only one coupling matrix H for the complete aircraft. In a next step, more FE points are used for the coupling, and the interpolation region is divided in equidistant partitions. In each partition, a separate matrix H^i is be generated and used corresponding to Eq. 2 for the load transformation. This procedure has been performed for 10 partitions and 762 coupling points, for 20 partitions and 1126 points, and finally using 250 partitions and 43422 points. In all cases, the direction of the partitions has been kept in y-direction, in order to obtain a local transfer of forces in each partition, especially on the wing. After the load transformation, the local momentum around the c/4 line of the right wing has been calculated to assess the quality of the momentum transfer in the coupling.

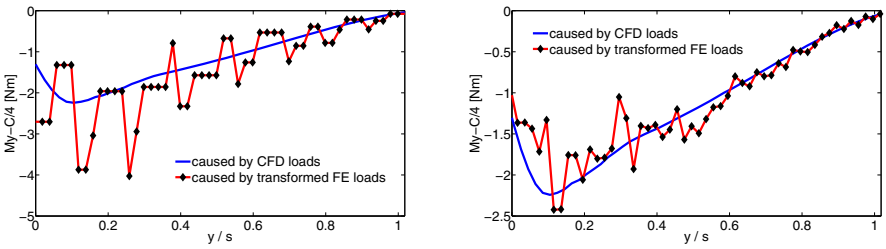

Fig. 9. Left: Momentum around the local c/4-line caused by the CFD loads and through the transformed FE loads using one coupling matrix and 199 coupling points. **Right:** Using 10 coupling matrices and 762 coupling points.

In Fig. 9 and Fig. 10 the results of the load transformation using the partitioning approach is depicted. The blue lines in the graphs show the local momentum around the c/4 line of the right wing caused by the aerodynamic forces on the CFD mesh. The black line with the delta symbols show the momentum caused by the transformed loads using one or more partitions and hence several coupling matrices H^i. Thus, in the first case, 199 coupling points are used in just

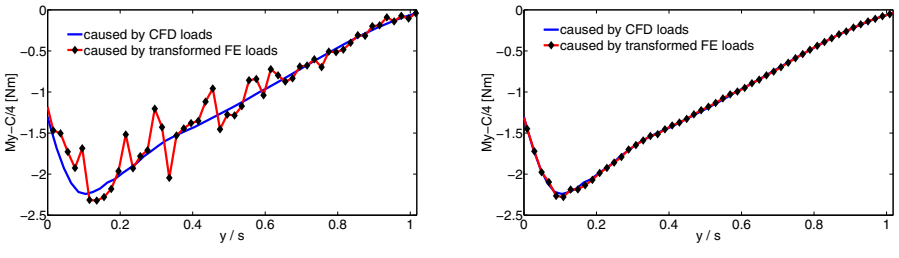

Fig. 10. Left: Momentum around the local c/4-line caused by the CFD loads and through the transformed FE loads using 20 partitions and 1126 coupling points. **Right:** Using 200 coupling matrices and 43422 coupling points.

one coupling matrix for the whole region. In the second case, 762 coupling points are used in 10 non-overlapping partitions in y-direction, each using separate coupling matrices. Likewise, the third case uses 1126 points and 20 partitions, and case four uses 43422 points and 250 partitions.

The comparison of the results shows well the local influence of the load transformation. One can observe, that with increasing number of supporting points, and using the partitioning approach in y-direction, the local forces and therefore also the local momentum around the c/4 line of the wing become more accurate. Using the whole FE model information (43422 points) produces the best agreement between the momentum caused by the aerodynamic forces and the momentum $M_{c/4}$ on the structure; the error between CFD forces and momentum and FE forces and momentum is very small, see the right picture in Fig. 10. The reason is, of course, that more coupling points allow more information to be transferred, resulting in a more precise transformation of the aerodynamic loads onto the structural points.

8 Conclusion

In this article a possible partitioning approach to solve the spatial coupling problem of large scaled industrial models has been presented. The approach has been validated for different partitioning strategies with respect to number and direction of the partitions. The obtained numerical results have been compared with experimentally determined wind tunnel data. It could be shown that the approach works very well and that all partitioning choices produce very similar results for the static aeroelastic equilibrium.

A few conclusions concerning the use of the partitioning approach for large models can be drawn. First, the analysis shows that automatic partitioning with overlap of the areas is a suitable choice for the handling of large models. The resulting coupling matrices are small, the simulation time for the determination of the coupling matrices and for the interpolation of deflections and the transfer of loads is reduced. Number and direction of the partitions did not have a significant influence on the reference model.

For the interpolation of deflections, another pragmatic approach for large models is the selection of a subset of coupling nodes on the FE side. For this method, it could be shown that the number of coupling points is not of large significance for the resulting deflection, provided that a sensible minimum number of points is selected. Furthermore, the points should be more or less equally distributed over the coupling region.

Concerning the loads transfer, small spanwise partitions without overlap are suggested. This way, the local error in force and momentum transfer can be minimized. As a consequence, it is not necessary to use the same partitions, and consequently not the same coupling matrices H and H^T for the interpolation of deflection and the transfer of forces between CFD and FE model. While for global coupling matrices H, the global equivalence of forces and moments is guaranteed, this might still lead to significant local errors. The use of small partitions can solve that problem.

Finally, while the findings in COMFLITE support the potential of automated treatment of large coupling models, it is still advisable to test the convergence of the coupling procedure for each new configuration. The current paper has provided criteria for such a test.

Acknowledgments. The authors would like to thank the colleagues of the Institute of Aerodynamics and Flow Technology, Braunschweig for their professional cooperation, particularly Dr. R. Heinrich and Dr. A.R. Hübner for the provision of the model geometry of the DLR-F12 wind tunnel model for the CFD mesh generation, the FE model and all the experimental data for the comparisons with the simulation results. The work presented has been funded in the framework of the project COMFLITE in the 4$^{\text{th}}$ German Nation Aeronautical Research Programme.

References

1. Beckert, A., Wendland, H.: Multivariate Interpolation for Fluid-Structure-Interaction Problems using Radial Basis Functions. AST - Aerospace Science and Technology, Art. No. 5125 (2001)
2. Schaback, R.: Creating Surfaces from Scattered Data Using Radial Basis Functions. Mathematical Methods for Curves and Surfaces. Vanderbilt University Press (1995) ISBN 8265-1268-2
3. Gneiting, T.: Radial Positive Definite Functions Generated by Euclid's Hat. Journal of Multivariate Analysis 69, 88–119 (1999)
4. Beckert, A.: Ein Beitrag zur Strömungs-Struktur-Kopplung für die Berechnung des aeroelastischen Gleichgewichtszustandes. DLR-FB No. 97-42, PhD-Thesis Göttingen (1997) (in German)
5. Harder, R.L., Desmarais, R.N.: Interpolation Using Surface Splines. AIAA Journal 9(2), 189–191 (1972)
6. Hounjet, M., Meijer, J.: Evaluation of Elastomechanical and Aerodynamic Data Transfer Methods for Non-planar Configurations in Computational Aeroelastic Analysis. In: Proceedings International Forum on Aeroelasticity and Structural Dynamics, Manchester, UK (1995)

7. Wendland, H.: Konstruktion und Untersuchung radialer Basisfunktionen mit kompaktem Träger. University of Göttingen, PhD-Thesis (1996) (in German)
8. Ahrem, R., Beckert, A., Wendland, H.: A New Multivariate Interpolation Method for Large-Scale Spatial Coupling Problems in Aeroelasticity. In: Conference Proceedings to the International Forum on Aeroelasticity and Structural Dynamics (IFASD), Munich (2005)
9. Wendland, H.: Fast Evaluation of Radial Basis Functions: Methods based on Partition of Unity. In: Chui, X.C.K., Schumaker, L.L., Stoeckler, J. (eds.) Approximation Theory, pp. 473–783. Vanderbilt University Press, Nashville (2002)
10. Ahrem, R.: Algorithmen zur Kopplung und Interpolation in der Aeroelastik. University of Göttingen, PhD-Thesis (2005) (in German)
11. Gardner, A.D., et al.: Adaptive load redistribution using mini-TED's. In: 25th International Congress of the Aeronautical Sciences (ICAS), Hamburg, Germany (2006)
12. Neumann, J., Nitzsche, J., Voss, R.: Aeroelastic Analysis by Coupled Non-linear Time Domain Simulation. RTO-AVT-154, Specialist's Meeting on Advanced Aeroelasticity, Loen Norway (2008)
13. Neumann, J., Ritter, M.: Steady and Unsteady Aeroelastic Simulations of the HIRENASD Wind Tunnel Experiment. In: IFASD - International Forum on Aeroelasticity and Structural Dynamics, Seattle, USA, June 21-24 (2009)
14. Löser, T., Hübner, A.R.: Influence of Wing Elasticity on Dynamic Derivatives of Transport Aircraft. In: 48th AIAA Aerospace Sciences Meeting, Orlando, Florida, USA, January 4-7 (2010)
15. Hübner, A.R., Kilian, T., Spiering, F.: Influence of Wing Elasticity on the Experimental and Numerical Determination of Dynamic Derivatives. In: STAB-Symposium, Berlin, Okt (2010)
16. Gerhold, T., et al.: Calculation of Complex Three-Dimensional Configurations Employing the DLR-TAU-Code. AIAA Journal 0167 (1997)
17. Dwight, R.: An Implicit LU-SGS Scheme for Finite-Volume Discretizations of the Navier-Stokes Equations on Hybrid Grids. DLR-FB-2005-05 (2005) ISSN 1434-8454
18. Spalart, P.R., Allmaras, S.R.: A One-Equation Turbulence Model for Aerodynamic Flows. AIAA Paper, No.92-0439 (1992)